Published in Physical Review B 69, issue 125117, 1-9, 2004
which should be used for any reference to this work

Pseudogapped Fermi surfaces of $1T$-TaS_2 and $1T$-$TaSe_2$: A charge density wave effect

M. Bovet,[1] D. Popović,[2] F. Clerc,[3] C. Koitzsch,[3] U. Probst,[4] E. Bucher,[4] H. Berger,[5] D. Naumović,[1] and P. Aebi[3]
[1]*Département de Physique, Université de Fribourg, Pérolles, CH-1700 Fribourg, Switzerland*
[2]*Experimentalphysik, Universität des Saarlandes, D-66123 Saarbrücken, Germany*
[3]*Institut de Physique, Université de Neuchâtel, CH-2000 Neuchâtel, Switzerland*
[4]*Fachbereich Physik, Universität Konstanz, D-78457 Konstanz, Germany*
[5]*Institut de Physique Appliquée, EPFL, CH-1015 Lausanne, Switzerland*

We report room temperature angle-resolved photoemission experiments on $1T$-TaS_2 and $1T$-$TaSe_2$ complemented by density-functional theory calculations. Fermi-surface mapping experiments in the charge-density wave (CDW) phase are similar for the two compounds and do not show symmetries due to the CDW-induced new Brillouin zones. However, the band structure a few eV below the Fermi level (E_F) displays a clear modulation that we relate, in both cases, to the CDW. At E_F, the spectral weight distribution reflects the band structure of the normal state, but no clear quasiparticle crossing is located. Near the zone center $\overline{\Gamma}$, CDW-split quasilocalized Ta dz^2 subbands are observed in the vicinity of E_F. For $1T$-TaS_2 and $1T$-$TaSe_2$, they are thermally populated slightly above E_F and close to E_F, respectively. The observed behavior can be understood in terms of the CDW reconstructed, spectral function weighted band structure.

I. INTRODUCTION

The pseudogap in high-temperature superconductors (HTS) is now regarded as a key property directly related to the mechanism behind superconductivity in these materials,[1] where an electronic instability drives the pseudogap and the remnant Fermi-surface (FS) behavior.[2] Recently, a pseudogap over large portions of the FS has been observed in angle-resolved photoemission (ARPES) experiments on the transition-metal dichalcogenide (TMD) $1T$-TaS_2 instead of a nesting induced partially removed FS in the charge-density wave (CDW) phase.[3] This new surprising property was questioned to be related to instabilities induced by the underlying Mott localization derived metal-insulator transition (MIT) (Ref. 4) at 180 K via fluctuations.[3] The isostructural $1T$-$TaSe_2$ with its identical CDW at RT appears to be the ideal candidate for further enlightening, as it does not exhibit a bulk MIT at lower temperatures. Very recent experiments, however, showed that $1T$-$TaSe_2$ exhibits a surface MIT.[5]

Even in the HTS, the origin of the pseudogap is still a topic of debate as to whether or not this pseudogap is a precursor of the actual gap in the electronic spectrum in the superconducting state below T_c.[6] Klemm[6] notices that the HTS pseudogap regime is strikingly similar to the one seen in TMD's and in some organic layered superconductors and proposes that the pseudogap in the HTS arises from CDW's and/or spin-density waves and not from superconducting fluctuations (or preformed pairs).

Despite their quite well-understood structural properties, studied by means of x-ray scattering,[7,8] the two $1T$-polytypes of the TaS_2 and $TaSe_2$ of the layered TMD's are also of strong interest in the debate on the mechanism behind the occurrence of the CDW, whose main feature is a starlike clustering (the so-called "stars of David") in the Ta plane [Fig. 1(c)].[9] The basic structure is sandwichlike: the hexagonal plane of Ta is sandwiched by two hexagonal S, respectively, Se sheets leading to a quasi-two-dimensional (2D) material. The quasi-2D character of the Fermi surface has been used to explain the CDW formation,[9] which induces the starlike distortion in the Ta plane. However, the x-ray scattering results show a three-dimensional reconstruction of the lattice by the formation of the CDW also along the c axis. In a previous publication,[10] we propose the necessary interplane coupling inbetween two sandwiches of $1T$-TaS_2 at RT to occur as a consequence of the *in-plane* CDW in the Ta layer. On the other hand, Horiba *et al.*[11] for $1T$-$TaSe_2$ conclude that the Fermi surface has three-dimensional character due to

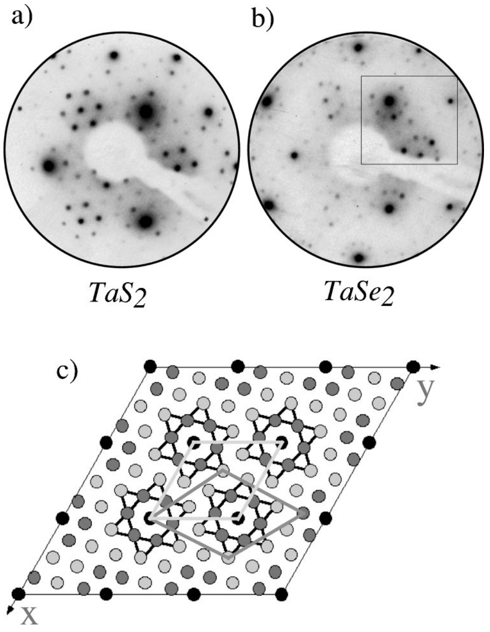

FIG. 1. Low-energy electron-diffraction patterns for $1T$-TaS_2 (a) and $1T$-$TaSe_2$ (b). In the Ta-plane, two CDW reconstructions may occur [inducing new superspots as emphasized with a square in (b)]; they are shown in (c). See text for more details.

a large charge transfer between Ta $5d$ and Se $4p$ orbitals. Last but not least, the debate on where to place a possible nesting vector on the FS contours, is still open. The structural evolution (induced by the CDW) with temperature T of the two materials shows considerable differences reflected in drastic differences in the resistivity curves. Undistorted at high T, $1T$-TaS$_2$ has a first phase transition at 850 °C (Ref. 7) yielding an incommensurate (IC) CDW phase. Below 350 K, the so-called nearly commensurate (NC) phase consists of commensurate (C) domains (73 Å diameter in average, with the stars of David) separated by incommensurate domain walls;[7,12] the abrupt resistivity jump at 350 K is followed by a semiconductinglike temperature behavior the resistivity slightly increases with decreasing temperature. Below a MIT at 180 K the system enters the C phase, characterized by a resistivity with an order of magnitude higher but, paradoxically, with metalliclike slope. The $1T$-TaSe$_2$ with its single phase transition at 473 K gets into the commensurate CDW phase (with the same symmetry as $1T$-TaS$_2$) with a sudden increase in the resistivity but still with metallic temperature behavior.

In the present paper, we give a detailed comparison of the Fermi surfaces of $1T$-TaS$_2$ and $1T$-TaSe$_2$ as measured by ARPES. The photoemission experiments analysis is complemented by density-functional theory (DFT) band structure calculations for both samples. The article is organized as follows. In Sec. II the experimental and computational details are outlined. Fermi-surface mapping and band mapping experiments are presented in Secs. III and IV, respectively. In Sec. V the analysis puts forward the role of the thermal occupation of bands implying differences in transport properties of both materials. Finally, after presenting the band structure of the realistic CDW distorted lattice (Sec. VI), the article ends with a discussion of the nesting vector (Sec. VII) and conclusions (Sec. VIII).

II. EXPERIMENT AND COMPUTATION

ARPES energy distribution curves (EDC's) and Fermi-surface mapping (FSM) measurements have been collected at RT in a modified VG ESCALAB Mk II spectrometer using monochromatized He I$\alpha(h\nu=21.2$ eV) photons.[13] The sequential motorized sample rotation has been outlined elsewhere.[14] The energy and angular resolution were 20 meV and $\pm 0.5°$, respectively. Pure $1T$-TaS$_2$ and $1T$-TaSe$_2$ samples were prepared by vapor transport[15,16] and cleaved *in situ* at pressures in the lower 10^{-10} mbar region. The accurate position of the Fermi level (E_F) has been determined on a polycrystalline copper sample. In some cases, the ARPES results have been normalized by the Fermi-Dirac function in order to bring to evidence states around the Fermi line. Cleanness and quality have been checked by x-ray photoelectron spectroscopy and by low-energy electron diffraction (LEED), respectively. Well-defined LEED superspots confirmed the presence of the CDW-induced reconstruction. X-ray photoelectron diffraction was used to determine the sample orientation *in situ* with an accuracy of better than 0.5°.

LEED results are shown in Figs. 1(a) and 1(b). Well-defined characteristic hexagonal spots of the basic structure are clearly present. Each of them is surrounded by those of the superstructure. For the $1T$-TaSe$_2$, however, more than one reconstruction is visible [Fig. 1(b), inset] due to two domains. Wilson *et al.*[9] performed electron micrographs of the Se alloy and also found different domains. They proposed dislocations in a single sandwich, i.e., twin boundaries formed by a Ta atom row separating α and β superlattice domains, rotated by, respectively, $\pm 13.54^{\mathrm{o}}$ with respect to the *undistorted* basic structure.[9] However, they did not show evidence of two domains in $1T$-TaS$_2$, neither the recent literature does which states the same observations.[7,8]

Band structure calculations have been done using the WIEN package implementing the FLAPW method within the framework of DFT.[17] For the exchange-correlation potential the generalized gradient approximation was used.[18] We considered the photoemission process in assuming a free-electron final state without introduction of any matrix elements effects.[19]

III. FERMI-SURFACE MAPPING

Since both compounds are isoelectronic (d^1 in the ionic picture) they are expected to give similar Fermi-surface maps. One has to keep in mind that an experimental FSM is not necessarily the actual FS, but a pattern reflecting the anisotropic distribution of the spectral weight of the electrons from the Fermi level. These patterns are shown in Figs. 2(a) and 2(b), mapped with respect to the conserved surface parallel component of the wave vector ($k_{\|}$). The first Brillouin zone (1BZ) has been drawn, as well as the crystallographic directions. The points of the images correspond to photoelectron intensities (gray scale, with high intensity in white) in an energy window around the Fermi level taken as a function of emission angle. The outer circle corresponds to grazing emission. The raw data shown in Fig. 2(a) has its high intensity in the 1BZ and is threefold and starlike. Its branches are more inequally weighted for the sulfide. At higher polar angles the intensity decreases but regains strength in the 2BZ (towards grazing emission). The features at high polar angles are difficult to distinguish as the gray scale has a limited dynamic range.

In order to enhance the information close to the grazing angles, the intensities have been normalized by the mean azimuthal value. In addition, mirror symmetry around the Γ-M axis has been applied to recover the crystal symmetry. In our experiment this mirror symmetry is broken since the unpolarized light comes in along a non-high-symmetry direction. The consequent strong, orbital dependent polarization effect has been outlined, e.g., for copper in Ref. 21. The influence of polarized light on such photoemission experiments has also been discussed in the literature for the $1T$-TaS$_2$, but only for normal light incidence.[20]

DFT calculations for the *undistorted* structure in Fig. 2(c) compared to the experiments taken at RT in the CDW phase in Fig. 2(b) clearly give evidence for the (1×1), i.e., *unreconstructed* character of the electronic structure. In both cases, the simulation is a superposition of two three-ellipse-like flowers, one rotated by 120° with respect to the other.

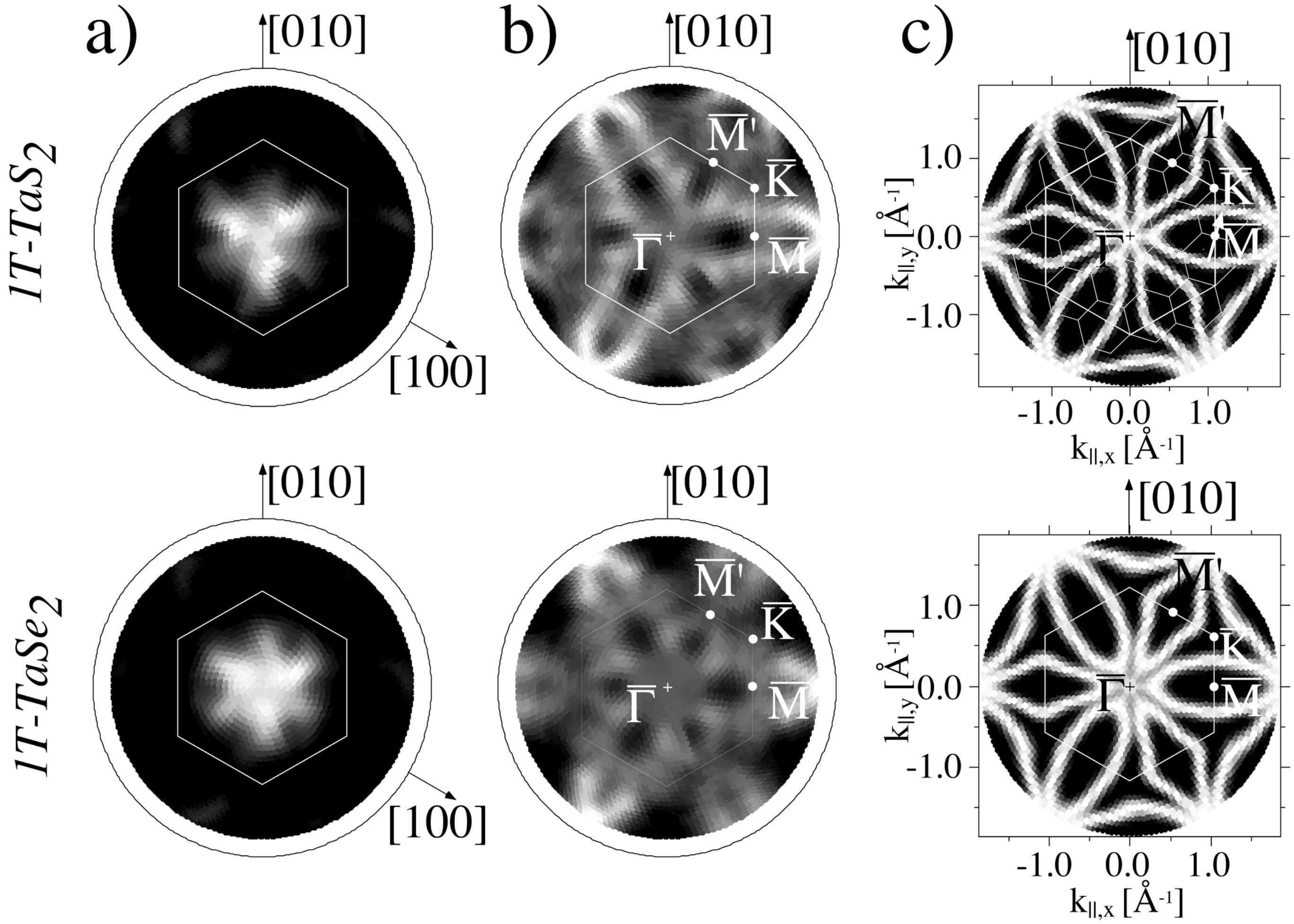

FIG. 2. Fermi-surface mapping with hexagonal unreconstructed hexagonal BZ's and high-symmetry points for both materials. Raw data (a) have been normalized by the mean azimuthal value (b). DFT simulations are given in (c). The $1T$-TaS$_2$ simulation has been added the CDW-induced reconstructed BZ's; a possible nesting vector is shown pointing across $\overline{M}$.

The fact that along $\overline{\Gamma}$-$\overline{M'}$ the ellipse gets a strong variation in going through the 1BZ gives a first indication for a weak $k_\perp$- dependence in the *unreconstructed* electronic structure of these quasi-2D materials. According to Ref. 20, the two flowers are subject to different selection rules in the photoemission process. The $\overline{\Gamma}$-$\overline{M}$ direction is preferred at E_F. Along $\overline{\Gamma}$-$\overline{M'}$, only the beginning of the ellipses is visible.

IV. ENERGY DISTRIBUTION CURVES

FSM is ideally complemented by EDC's to figure out the role of the underlying band dispersion. The comparison of the experiment with the calculation for the *undistorted* structure, up to a binding energy of 2 eV, is the theme of Fig. 3 We focus on the $\overline{\Gamma}$-$\overline{M}$ direction. As outlined already in an early calculation,[22] one recognizes the Ta $5d$ band. In both, disulfide and diselenide, the band forms a small holelike pocket close to $\overline{\Gamma}$ followed by a large electronlike pocket around $\overline{M}$. For $1T$-TaS$_2$, there is practically no hybridization with the S $3p$. However, for $1T$-TaSe$_2$ at Γ and M, the Se $4p$ orbitals get very close to the Ta band. Here, introduction of spin-orbit coupling in the calculation (not shown here) even yields crossing bands. This DFT description illustrates that the Ta $5d$ and Se $4p$ wave functions overlap and hybridize, while in the disulfide the Ta $5d$ band is isolated and solely drives the electrical properties. And this hybridization[11] might play a crucial role in understanding the differences in transport properties of these two materials, as outlined in Secs. V and VIII. On the ARPES EDC's (Fig. 3) the reader immediately sees that the photoemission intensities, despite the superstructure as detected by x-ray diffraction and LEED, still keep the band dispersion of the (1×1) *undistorted* crystal.

We now begin to analyze in detail the spectral weight around the Fermi energy using the symmetrization procedure,[23,24] first along the high-symmetry directions $\overline{\Gamma}$-$\overline{M}$ and $\overline{\Gamma}$-$\overline{K}$, then on azimuthal EDC's measured at polar angles of 20° and 32° (see further on FSM of Fig. 5 for location in surface reciprocal space). The goal is to determine whether there is a pseudogap or a band (quasiparticle) crossing at the Fermi energy. The symmetrization method is a common practice in the cuprates to infer whether the spectral function

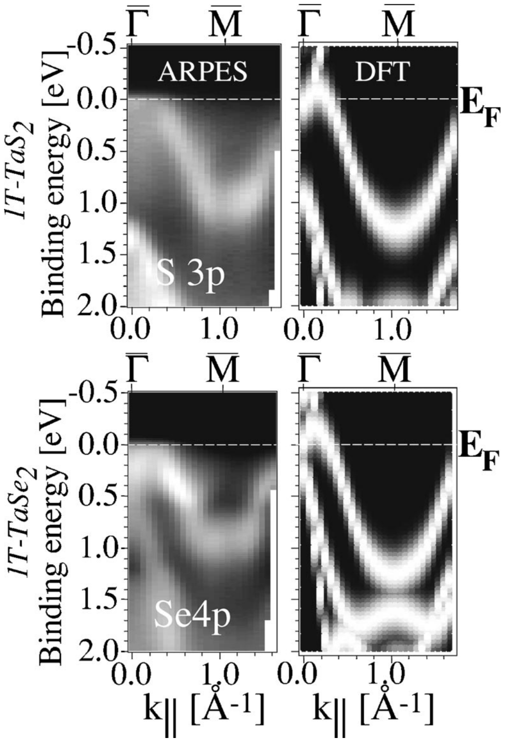

FIG. 3. ARPES and DFT energy distribution curves. See text for details.

peak crosses the chemical potential.[23,24] The idea of this symmetrization around E_F (or $\omega=0$) is to remove the perturbative effect of the Fermi-Dirac distribution cuttoff with the intrinsic temperature dependence of the spectral function $A(k_F,\omega,T)$ and it is shown[24] to be efficient even for weakly dispersive bands at E_F. The photoemission intensities of a spectrum are symmetrized with respect to E_F $(\omega=0)$ and summed. In practice, $\vec{k}_F$ is then identified as the boundary in momentum space between where symmetrized data have a dip (local minimum) and where they exhibit a peak (local maximum) at $\omega=0$.[24] It is related to the fact that, when approaching E_F, the quasiparticle peak progressively brings spectral weight closer to it. As soon as it is not any more occupied (crossing has occurred), a dip is seen in the symmetrized data.

The measurements shown above, (Fig. 3), done on a large polar angle range (50°), show enhanced spectral weight at E_F close to $\overline{\Gamma}$. The EDC's of Fig. 4 were all done along a high-symmetry direction crossing $\overline{\Gamma}$ (either $\overline{\Gamma}$-$\overline{M}$ or $\overline{\Gamma}$-$\overline{K}$). The spectra were taken every degree up to 1 eV binding energy. The spectrum plotted in bold has been measured at the normal ($\overline{\Gamma}$). Adjacent to the EDC's are the symmetrized curves. Along $\overline{\Gamma}$-$\overline{M}$ [Fig. 4(a)], the symmetrization for the disulfide leads to a peak, which gradually grows from 10° approaching the normal. Along the other direction [Fig. 4(b)], the scheme is the same, but starting from $\approx 16°$. We notice that no clear dip follows the peak, as it would be expected in order to be identified as a clearly crossing band. For the considered directions, the diselenide seems to be more pseudogapped as judged from the symmetrization peak

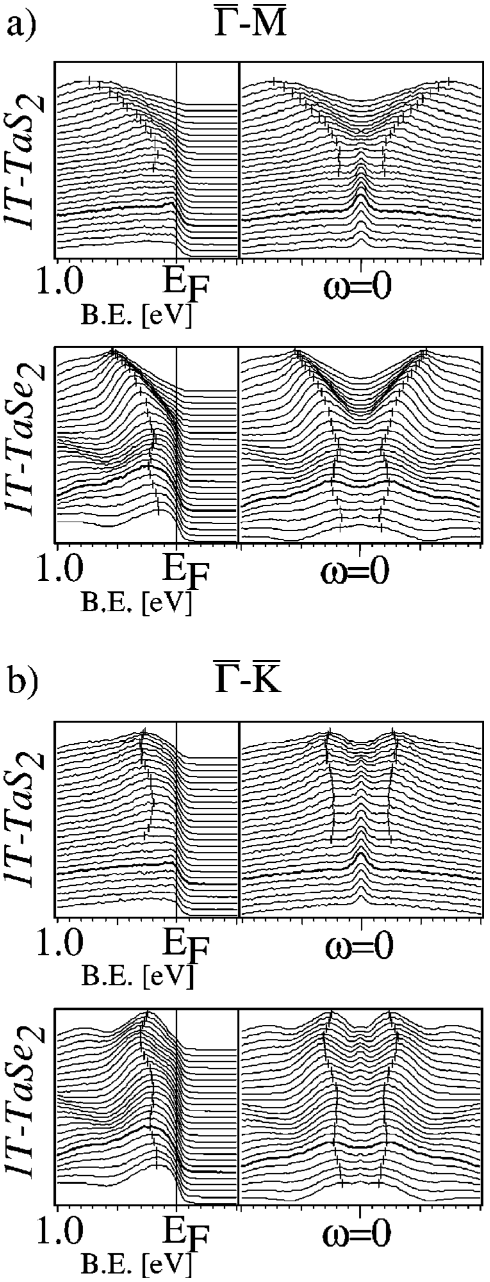

FIG. 4. On the left, spectra along two high symmetry directions, $\overline{\Gamma}$-$\overline{M}$ (a) and $\overline{\Gamma}$-$\overline{K}$ (b) across the normal emission (bold spectrum). Symmetrized data are shown on the right. See text.

in Fig. 4(a). Along $\overline{\Gamma}$-$\overline{K}$ in Fig. 4(b) the situation is similar and it is difficult to infer any crossing at the Fermi level. Nevertheless symmetrization peaks exist, confined in a circular region of about 20° centered at the normal. In the above discussions, the quasiparticle crossing was thought to occur starting from the occupied part of the band structure. It may be reasonable to envisage bands approaching E_F from the unoccupied states, then only dispersing a few meV into the occupied part.

The EDC's displayed in Fig. 4 range up to ≈ 0.67 Å^{-1} for the $1T$-TaS$_2$ and 0.65 Å^{-1} for $1T$-TaSe$_2$ in Fig. 3(a). In this range, the calculation proposes a regular crossing of the Ta

$5d$ band, in contrast to the experiment. In Fig. 4, we put small bars on the peaks of the dispersing band. For the S alloy, the dispersion is as expected, except that the band surprizingly folds back to higher binding energy after having approached the Fermi level. Along the $\bar{\Gamma}$-$\bar{K}$ direction the dispersion is clearly oscillating. This modulation is even stronger for the diselenide. It indicates that the dispersion of the apparently *unreconstructed* band structure contains oscillating features due to the CDW.

We measured further EDC's but scanning azimuthal angles in order to probe the spectral weight at E_F off normal but also away from the high-symmetry directions. Both samples clearly exhibit the same pseudogap. The $1T$-TaSe$_2$ measurements in Fig. 5 ($1T$-TaS$_2$ measurements are not shown) do not give evidence for spectral weight comparable to the one mentioned at low polar angles (Fig. 4). Half a FSM—normalized by the mean azimuthal value—is shown as an orientation guide. The first EDC's [Fig. 5(a)] were taken at polar angle of 20° as pointed out by the white arrow on the FSM. The black arrow indicates the order in which the spectra have been collected. The symmetrized results do not have a peak at $\omega = 0$, but the spectral weight is not zero. Therefore we have a pseudogap. The situation is very similar for the polar angle of 32° [Fig. 5(b)].

We simulated the EDC's of Fig. 5(a) with DFT [Fig. 5(c)] between the $\bar{\Gamma}$-$\bar{M}$ to the $\bar{\Gamma}$-$\bar{M}'$ directions. There is one band which is electronlike around the high-symmetry directions $\bar{\Gamma}$-$\bar{M}$ and $\bar{\Gamma}$-$\bar{M}'$. These pockets are recognizable in Fig. 5(a), but here two subbands disperse. These two flat subbands have also been measured by Horiba *et al.*[25] along the Γ ALM plane and are explained as a consequence of the CDW formation according to the calculation of Smith *et al.*[26] They are also present at 32° [Fig. 5(b)] the first subband closer to E_F seems to have decreased intensity with respect to the second one. The conclusions for $1T$-TaS$_2$ are similar, with the difference that the two subbands are less marked or have the trend to form a single broad peak. But these less marked features are meaningful taking into account that the disulfide at RT is composed by C domains among IC domain walls (where the CDW phase is changing). Then the CDW features in the band structure have to be less pronounced and disturbed by the changing phase in the domain walls[7] of the incommensurations.

The calculation for the *undistorted* structure in Fig. 3 shows a clear crossing close to $\bar{\Gamma}$. But the experiment does not. We cannot, in conclusion, claim to observe a quasiparticle crossing the Fermi level despite the presence of the symmetrization peak close to the central region. The symmetrization peak shows angular dependence, and the pseudogap seems to grow with larger polar angle.

V. THERMAL OCCUPATION AND TRANSPORT PROPERTIES

Before coming to an interpretation and a deeper understanding of the different subbands and the pseudogap via band structure calculations in Sec. VI, we proceed with a further analysis of states close to E_F. For analyzing intensities in the vicinity of E_F, i.e., for states which are thermally excited, the spectra are divided by the Fermi-Dirac function (FD). In Fig. 6(a), the normal emission spectrum is shown. The spectra are cut at about 140 meV ($5k_BT$) above the chemical potential. The resulting FD normalized spectrum is represented by small crosses. In (b), the dispersion of peaks has been outlined by circles, which have been positioned by hand on the maxima of the spectral intensities. Both TMD's show a very flat dispersion close to zero binding energy in the polar angle range near $\bar{\Gamma}$. For $1T$-TaS$_2$ the states lie slightly above the Fermi edge, whereas for $1T$-TaSe$_2$, they are straddling E_F. This may be of importance for the transport properties; the disulfide needs thermal activation, like in

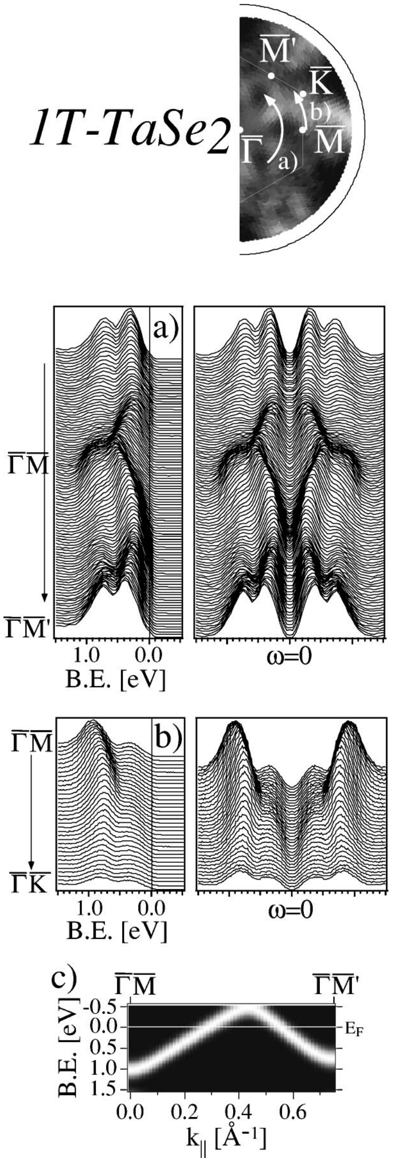

FIG. 5. Spectra taken along azimuthal angles on $1T$-TaSe$_2$ for two polar angles, respectively, 20° (a) and 32° (b). Their corresponding location in surface reciprocal space is given with the arrows on the FSM. Both were symmetrized (b) and (e); we note here that, although no peak appears, at $\omega = 0$, spectral weight is still present. It does not fall to zero. (c) Shows simulation for scanning at 20°.

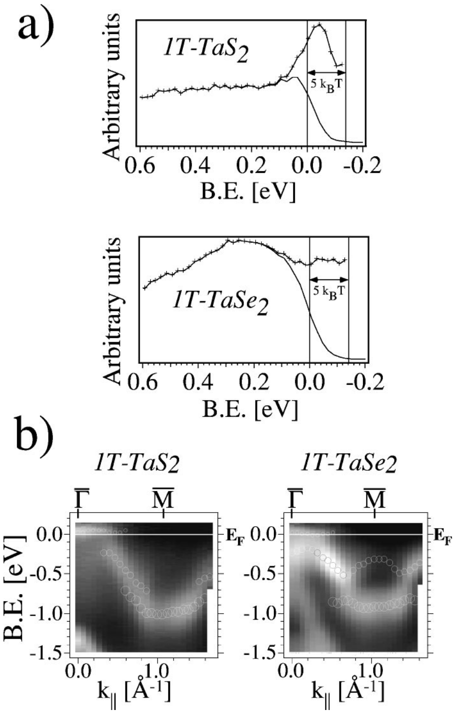

FIG. 6. Analysis of thermally excited states around E_F. Normal emission spectra are given in (a). The experimental spectrum is divided with the appropriate Fermi-Dirac function to reveal the thermally excited bands (crossed line). In (b), one sees the dispersion over the whole scanning range. Circular markers emphasize the splitting of the Ta band.

a semiconductor. The Se alloy has similar thermal occupation, but still with a band at E_F. Both samples, because of the CDW formation, have an increase in resistivity, however with intriguing different slopes as a function of T at RT. The above photoemission considerations are here consistent with the semiconductinglike slope (negative) of the $1T$-TaS$_2$ and the metalliclike one (positive) of the $1T$-TaSe$_2$.

Figure 6(b) also shows the Ta $5d$ band on its full energy range. We placed on each local maxima of the spectra the circular markers. Both materials reveal, once more, a modulated dispersion with stronger intensities according to the (1×1) BZ. The Ta band appears clearly split, and the subbands tend to oscillate. This observation of fine modulated structures is more evident on the $1T$-TaSe$_2$. We see the first subband (at low binding energies) on the complete polar angle range, the second one is more flat.

VI. REALISTIC RECONSTRUCTED BAND STRUCTURE OF 1T-TaS$_2$

A deeper understanding of the subbands may be obtained via a DFT calculation (as illustrated in Fig. 7), now computing not only the basic hexagonal structure but by considering the atomic displacements of the atoms as induced by the CDW in the $1T$-TaS$_2$ and measured by means of x-ray scattering.[7] For the band structure calculation, an approximate commensurate $(\sqrt{13}\times\sqrt{13}\times3)$ superstructure was derived from the refined structural coordinates of the incommensurate structure of the NC phase [notice that $\times3$ in this $(\sqrt{13}\times\sqrt{13}\times3)$ superstructure means that the unit cell contains 3 TaS$_2$ sandwiches]. The bottom of this trigonal *distorted* unit cell contains the center of the ‘‘stars of David’’ as shown on Fig. 1(c). A detailed explanation is given in Ref. 10. For the DFT computation, only the first sandwich [as shown in Fig. 1(c)] around $z=0$ was taken. The result is shown by dotted lines in Fig. 7(a) and is commented in detail in Ref. 10. The *reconstructed* band structure is plotted versus a path in the *unreconstructed* hexagonal reciprocal space. The correspondence between surface and bulk BZ’s is illustrated in Fig. 7(b). In Fig. 7(e) both surface *reconstructed* (13.9° rotated hexagonal lattice, with positive rotation as observed on the LEED pattern) and *unreconstructed* (large hexagon) BZ’s have been drawn with lines. A band character analysis indicates that the first seven subbands below the Fermi energy [Fig. 7(a)] are due to the Ta atoms. Thus the Ta $5d$ band is split by the CDW formation. We here emphasize the presence of the uppermost flat subband in the central plane of the 1BZ and its dispersion in z along Γ-A. It moves off from the underlying subbands, and oscillates around E_F at the border of the BZ (along $A-L$). This band has mostly dz^2 character.

Figure 7(c) shows the simulated EDC as issued from the *reconstructed* unit cell. A free-electron photoemission final state, as plotted in Fig. 7(d), is assumed to determine the k points within the BZ. We can identify the six subbands, and the uppermost seventh subband straddling E_F only coming down from E_F after 1.5 Å^{-1}. It is a cut in the *reconstructed* (r) reciprocal space. The free-electron final state is shown up to 60°, the polar angle range we took for the simulation of the EDC [Fig. 7(d)]. (A thick line was chosen for the Fermi energy and a thin one for a binding energy of 2 eV.) At the normal, the measured k points are closer to A than to Γ, but reach the center of the BZ at 60°. This z dispersion from A to Γ can be related to Fig. 7(a), in particular, when looking at the uppermost subband. It is the same dispersion as on the EDC [Fig. 7(c)]. Furthermore, according to the experimental bandwidth on the EDC (Fig. 3) (up to 1.3 eV), we have the confirmation that our photoemission experiments on the $1T$-TaS$_2$ probe the BZ off center plane. This would also practically not be affected by a slight change of our estimated inner potential (13 eV). It would just induce a small shift of the final state, which still would stay closer to A than to Γ. And the same can be stated for the $1T$-TaSe$_2$, since the c-axis lattice constant is very similar. On the calculated EDC [Fig. 7(c)], the points at E_F are exactly those plotted along Γ-M on the *reconstructed* simulated FSM of Fig. 7(e). Just after Γ [going along Γ-M in Fig. 7(c)], the Fermi line of the EDC is twice crossed by the flat subband. The crossing of this subband at E_F forms the ‘‘flowers’’ paved FSM in Fig. 7(e). The ‘‘flowers’’ clearly follow the grid of the *reconstructed* higher BZ’s, and [in Fig. 7(e)] we guess also the crossing of the seventh flat subband moving down when looking along Γ-M in the *unreconstructed* 2BZ. As a matter of fact, this crossing is seen as a white circle close to the border of Fig. 7(e).

Experimentally we observed subbands and confirmed

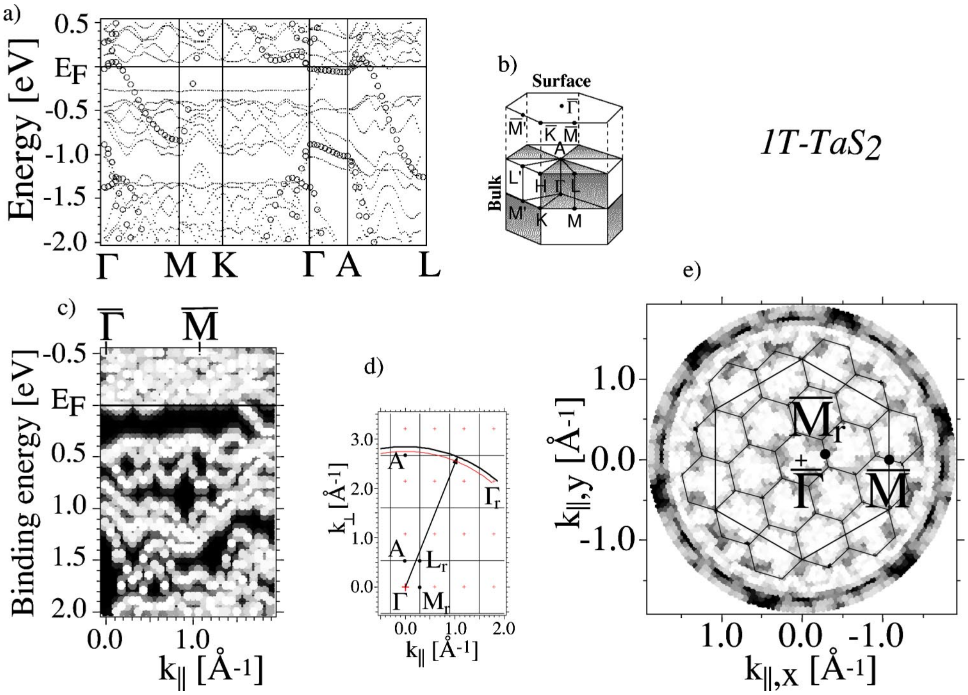

FIG. 7. Result from calculations for the *distorted* structure. (a) Band structure along high-symmetry lines, circular markers correspond to calculations for the undistorted structure. (b) Bulk surface BZ's correspondence. (c) Simulation of an EDC along Γ-M for He I. (d) Cut in reciprocal space with free-electron final-state wave vector for He I. (e) Simulation of FSM with reconstructed BZ's.

theoretically the formation of subbands by the CDW. Despite the presence of flat subbands all over the BZ, the photoemission intensities are rather distributed according to the *unreconstructed* band structure (Figs. 2 and 3). For the 1T-TaS$_2$ the influence of the CDW induced new BZ's is not observed in the literature,[27–29] although at RT in the NC phase domains of $\approx$70 Å size exist with a structure corresponding to the C phase.[7,12] We here state the same for the 1T-TaSe$_2$. Clearly, the calculations using the reconstructed structure do not reproduce the observed experimental intensity distributions displayed in Figs. 2(b) and 3. Certainly, the calculations using the *unreconstructed* structure [Figs. 2(c) and 3] fit much better. In order to understand this we need an important other ingredient.

Recently, Voit *et al.*[30] have modeled the spectral weight distribution of tight-binding electrons in a solid with competing periodic potentials as in the case of CDW superstructures. They show that the dispersion of the eigenvalues (band structure) follows the *reconstructed* BZ's, but the spectral weight (proportional to the photoemission intensity) is concentrated along the extended zone scheme dispersion of the *nonreconstructed* BZ, i.e., it follows the *unreconstructed* band structure. In Fig. 7(a), we plotted empty circles along the (1×1) dispersion of the disulfide. Accordingly, the experimental intensities are supposed to populate the underlying subbands following the unreconstructed bands and that is what we observed in the EDC's of Figs. 2–6.

Therefore, we are now able to obtain a detailed understanding of our measurements and of the electronic structure of these compounds. The CDW induces a profound reconstruction of the band structure. For a simple understanding, the formation of stars of 13 Ta atoms [Fig. 1(c)] (with one electron each, in an ionic picture) leads to seven subbands with two electrons per band except for the top one which is only half filled. The calculation of Fig. 7(a) where we see the seven subbands along $\Gamma MK\Gamma$ between 0.2 and 1.0 eV binding energy confirms this view. The top-most seventh band (which is due to the star center Ta atom) crosses E_F along Γ-A confirming the partial occupation. Furthermore, considering the star of 13 Ta atoms being composed of the central atom surrounded by a first shell of 6, almost equivalent, nearest neighbors and a second shell of six, almost equivalent, next nearest neighbors we may group the subbands in three manifolds. Nearest and next nearest neighbors are represented by a manifold containing three subbands each and the third manifold only contains the top-most subband due to the star center atom. These three manifolds are clearly separated along $A-L$ as seen in Fig. 7(a) and also in the simulation [Fig. 7(c)]. The top-most manifold or subband is straddling E_F.

Going back to Fig. 6(b) we can identify the three manifolds with their intensity given by the spectral function following, according to Voit *et al.*,[30] the nonreconstructed band structure (see Fig. 3). In principle, the subband at E_F is present all over the BZ. Its observation in ARPES, however, depends on its position with respect to E_F (above or below while straddling E_F, see Figs. 7(a) and 7(c) and on the spectral function which favors the unreconstructed band structure.

In fact, the oscillating behavior of the top-most subband is displayed in Fig. 7(e) for the complete BZ. As a consequence we may explain our FSM experiments [Fig. 2(b)] in terms of the (1×1)-unreconstructed FS [Fig. 2(c)] weighted with the oscillating behavior of the top-most subband. Furthermore this top-most subband has predominantly dz^2 character which explains the strong intensity drop via matrix elements for higher emission angles. This intensity drop (and therefore the matrix element effect) has been removed when going from Fig. 2(a) to Fig. 2(b), flattening the intensity plot.

The above is in accordance with our observations of a pseudogap. As mentioned above, the top-most subband is present all over the BZ. Even along $\Gamma MK\Gamma$ empty states are very close to E_F, everywhere. For this reason we are always finding spectral weight at E_F, whether it is originating from thermal occupation via the Fermi-Dirac distribution or whether states are truly below E_F. However, since these states are merely straddling E_F, we cannot observe a true crossing of a quasiparticle peak and hence experience a pseudogap behavior displaying an intensity distribution of the spectral weight according to the spectral function with (1×1) symmetry.

We complete the room-temperature considerations in this section with a brief speculation concerning the surface MIT recently found in $1T$-TaSe$_2$ at low temperature by Perfetti *et al.*[5] The new CDW-induced BZ's have lead to flattened backfolded bands, i.e., the CDW modulated electronic density has reduced the bandwidth W. This certainly reduces the (W/U) parameter (U, the onsite Coulomb energy), which is crucial for understanding the activation of a Mott MIT.[5] In $1T$-TaS$_2$ at room temperature, the thermal occupation was proposed to act as in a semiconductor, which is confirmed by the semiconductinglike slope of the resistivity. As a consequence, there is a temperature where the thermal excitation is not sufficient anymore to create enough charge carriers. Possibly, it corresponds to the beginning of the Mott MIT. At this temperature, screening is lowered again (it was already decreased with the introduction of CDW induced new BZ's and corresponding backfolding of bands) and delivers the necessary favorable conditions for the Mott transition to develop for both bulk and surface.

On the other hand, for metallic $1T$-TaSe$_2$, the interplay U-W is differently balanced due to the stronger overlap of Ta $5d$ and Se $4p$ derived bands. This hybridization tends to increase W, establishing unfavorable conditions for a phase transition. However, a reduced coordination number as it is the case at the surface, could be decisive to reduce W specifically at the surface. This is proposed by Perfetti *et al.*[5] reporting such a surface MIT in the Se compound by comparing ARPES and dynamical mean-field theory calculation of the spectral function of a half-filled Hubbard model. Below this transition, however, there is still spectral weight remaining at E_F with a possible contribution from the underlying bulk states. Two mechanisms would then explain the behavior, one as a consequence of the other. At room-temperature electron-phonon coupling is at work and the CDW modulated states are responsible for the RT pseudogap formation (see above). On top of the CDW-induced, reduced carrier density, as the temperature is lowered, electron-electron correlation sets in at the surface and leads to the transition.[5]

VII. THE NESTING VECTOR

The distribution of the spectral weight follows the unreconstructed band dispersion. On the search for the origin of the CDW we are looking at the unreconstructed FS contours to find possble portions that are removed because of favorable nesting conditions. The unreconstructed Fermi-surface contours have an elliptic shape with rather flat sections close to the M point (Fig. 2). This offers the possibility to connect these flat parts of the contours on both sides of the M point according to a quasi-one-dimensional model with long parallel sections of the FS undergoing a Peierls transition. The length and direction of a possible nesting vector $\vec{q}_{CDW}$ appears favorable (see small white arrow in Fig. 2(c)). However, the idea behind the Peierls transition in a quasi-one-dimensional system is to bring the BZ boundary to lie on top of the flat parts of the FS contour. This is not happening in our case. We do not have a quasi-one-dimensional system but it is quasi-2D with threefold symmetry. Therefore, the system has to adopt a different strategy. By choosing a relatively long wavelength for the lattice distortion the new BZ's become relatively small, thus introducing a large number of new zones cutting the FS contours many times. Yet, this might not be enough to account for the elastic energy needed to distort the lattice. But there is another (favorable) consequence of enlarging the unit cell, namely the splitting of bands due to inequivalent positions of identical atoms, i.e., the splitting of the single Ta 5d band into seven subbands. In our case the system managed to lower six of the seven subbands (i.e., almost all) completely below E_F, certainly resulting in a major energy gain.

VIII. CONCLUSIONS

We have shown that in addition to $1T$-TaS$_2$ also $1T$-TaSe$_2$ is pseudogapped. The CDW which has identical symmetry for the two compounds is found to be responsible. A detailed analysis of the band structure of both materials, as observed by photoemission with He $I\alpha$ radiation, reveals CDW split features which are confirmed by realistic *ab initio* DFT calculations, whose unit cell accounts for the atomic displacements due to the CDW formation. As a matter of fact, the CDW induced lattice distortion splits the Ta $5d$ band into subbands. It appears that only one of the subbands is close to E_F, the others being located below, herewith stabilizing the CDW structure. The subband close to E_F is straddling the Fermi level and is responsible for the observed pseudogap behavior since it does not exhibit a clear quasiparticle crossing in the ARPES spectra but is creating persistent spectral weight at E_F. In addition, the spectral function is modulating the ARPES intensities according to the unreconstructed band structure, explaining the apparent absence of spectral features due to the new BZ's in FSM's and band-mapping experiments. As a consequence, this indicates that the pseudogap is not related to possible fluctuations of the underlying MIT as presumed previously.

ACKNOWLEDGMENTS

Skillful technical assistance was provided by E. Mooser, O. Raetzo, R. Schmid, Ch. Neurурer, and F. Bourqui. We are grateful to S. van Smaalen who provided the coordinates of the atomic positions to perform the DFT calculation of the CDW reconstructed case. This project has been supported by the Fonds National Suisse de la Recherche Scientifique.

[1] H. Ding, T. Yokoya, J.C. Campuzano, T. Takahashi, M. Randeria, M.R. Norman, T. Mochiku, K. Kadowaki, and J. Giapintzakis, Nature (London) **382**, 51 (1996); A.G. Loeser, Z.-X. Shen, D.S. Dessau, D.S. Marshall, C.H. Park, P. Fournier, and A. Kapitulnik, Science **273**, 325 (1996).

[2] F. Ronning, C. Kim, D.L. Feng, D.S. Marshall, A.G. Loeser, L.L. Miller, J.N. Eckstein, I. Bozovic, and Z.-X. Shen, Science **282**, 2067 (1998).

[3] Th. Pillo, J. Hayoz, H. Berger, M. Grioni, L. Schlapbach, and P. Aebi, Phys. Rev. Lett. **83**, 3494 (1999).

[4] P. Fazekas and E. Tosatti, Philos. Mag. B **39**, 229 (1979); Physica B **99**, 183 (1980).

[5] L. Perfetti, A. Georges, S. Florens, S. Biermann, S. Mitrovic, H. Berger, Y. Tomm, H. Höchst, and M. Grioni, Phys. Rev. Lett. **90**, 166401 (2003).

[6] R.A. Klemm, Physica C **348**, 839 (2000).

[7] A. Spijkerman, Jan L. de Boer, Auke Meetsma, Gerrit A. Wiegers, and Sander van Smaalen, Phys. Rev. B **56**, 13 757 (1997).

[8] G.A. Wiegers, J.L. de Boer, A. Meetsma, and S. van Smaalen, Z. Kristallogr. **216**, 45 (2001).

[9] J.A. Wilson, F.J. Di Salvo, and S. Mahajan, Adv. Phys. **24**, 196 (1975).

[10] M. Bovet, S. van Smaalen, H. Berger, R. Gaal, L. Forró, L. Schlapbach, and P. Aebi, Phys. Rev. B **67**, 125105 (2003).

[11] K. Horiba, K. Ono, J.H. Oh, T. Kihara, S. Nakazono, M. Oshima, O. Shiino, H.W. Yeom, A. Kakizaki, and Y. Aiura, Phys. Rev. B **66**, 073106 (2002).

[12] X.M. Wu and C.M. Lieber, Science **243**, 1703 (1989).

[13] Th. Pillo, L. Patthey, E. Boschung, J. Hayoz, P. Aebi, and L. Schlapbach, J. Electron Spectrosc. Relat. Phenom. **97**, 243 (1998).

[14] P. Aebi, J. Osterwalder, P. Schwaller, L. Schlapbach, M. Shimoda, T. Mochiku, and K. Kadowaki, Phys. Rev. Lett. **72**, 2757 (1994).

[15] B. Dardel, M. Grioni, D. Malterre, P. Weibel, Y. Baer, and F. Lévy, Phys. Rev. B **45**, 1462 (1992).

[16] B. Dardel, M. Grioni, D. Malterre, P. Weibel, Y. Baer, and F. Lévy, Phys. Rev. B **46**, 7407 (1992).

[17] P. Blaha, K. Schwarz, and J. Luitz, computer code WIEN97 (Karlheinz Schwarz, Techn. Universität Wien, Austria, 1999), ISBN 3-9501031-0-4.

[18] J.P. Perdew, K. Burke, and M. Ernzerhof, Phys. Rev. Lett. **77**, 3865 (1996).

[19] Here, different values for both work function and inner potential were tested; however no relevant changes came out, as a consequence of the quasi-two-dimensional character of these materials.

[20] T. Matsushita, S. Imada, H. Daimon, T. Okuda, K. Yamaguchi, H. Miyagi, and S. Suga, Phys. Rev. B **56**, 7687 (1997).

[21] P. Aebi, J. Osterwalder, R. Fasel, D. Naumović, and L. Schlapbach, Surf. Sci. **307-309**, 917 (1994).

[22] H.W. Myron and A.J. Freeman, Phys. Rev. B **11**, 2735 (1975).

[23] M.R. Norman, H. Ding, M. Randeria, J.C. Campuzano, T. Yokoya, T. Takeuchi, T. Takahashi, T. Mochiku, K. Kadwaki, P. Guptasarma, and D.G. Hinks, Nature (London) **392**, 157 (1998).

[24] J. Mesot, M. Randeria, M.R. Norman, A. Kaminski, H.M. Fretwell, J.C. Campuzano, H. Ding, T. Takeuchi, T. Sato, T. Yokoya, T. Takahashi, I. Chong, T. Terashima, M. Takano, T. Mochiku, and K. Kadowaki, Phys. Rev. B **63**, 224516 (2001).

[25] K. Horiba, Kanta Ono, Han Woong Yeom, Yoshihiro Aiura, Osamu Shiino, Jin Ho Oh, Takayuki Kihara, Shinsuke Nakazono, Masaharu Oshima, and Akito Kakizaki, Physica B **284**, 1665 (2000).

[26] N.V. Smith, S.D. Kevan, and F.J. Di Salvo, J. Phys. C **18**, 3175 (1985).

[27] R. Claessen, B. Burandt, H. Carstensen, and M. Skibowski, Phys. Rev. B **41**, 8270 (1990).

[28] Th. Pillo, J. Hayoz, H. Berger, F. Lévy, P. Aebi, and L. Schlapbach, J. Electron Spectrosc. Relat. Phenom. **101-103**, 811 (1999).

[29] Th. Pillo, J. Hayoz, H. Berger, R. Fasel, L. Schlapbach, and P. Aebi, Phys. Rev. B **62**, 4277 (2000).

[30] J. Voit, L. Perfetti, F. Zwick, H. Berger, G. Margaritondo, G. Grüner, H. Höchst, and M. Grioni, Science **290**, 501 (2000).